Applied Materials Today 20 (2020) 100697

Contents lists available at ScienceDirect

Applied Materials Today

journal homepage: www.elsevier.com/locate/apmt

2D Germanane Derivative as a Vector for Overcoming Doxorubicin Resistance in Cancer Cells

Michaela Fojtů[a], Jan Balvan[b,e], Martina Raudenská[b], Tomáš Vičar[b], Jiří Šturala[a], Zdeněk Sofer[a], Jan Luxa[a], Jan Plutnar[a], Michal Masařík[b,e,g], Martin Pumera[a,c,d,f,*]

[a] Center for Advanced Functional Nanorobots, Department of Inorganic Chemistry, Faculty of Chemical Technology, University of Chemistry and Technology in Prague, Technická 5, Prague 16628, Czech Republic
[b] Department of Physiology, Faculty of Medicine, Masaryk University, Kamenice 5, Brno 62500, Czech Republic
[c] Department of Chemical and Biomolecular Engineering, Yonsei University, 50 Yonsei-ro, Seoaemun-gu, Seoul 03722, South Korea
[d] Future Energy and Innovation Laboratory, Central European Institute of Technology, Brno University of Technology, Purkyňova 656/123, Brno 61600, Czech Republic
[e] Department of Pathological Physiology, Faculty of Medicine, Masaryk University, Kamenice 5, Brno 62500, Czech Republic
[f] Department of Medical Research, China Medical University Hospital, China Medical University, No. 91 Hsueh-Shih Road, Taichung, Taiwan
[g] BIOCEV, First Faculty of Medicine, Charles University, Průmyslová 595, Vestec 25250, Czech Republic

ARTICLE INFO

Article history:
Received 2 April 2020
Revised 7 May 2020
Accepted 9 May 2020

Keywords:
2D materials
4-carboxybutylgermanane
germanane
targeted drug delivery
doxorubicin
ovarian cancer
drug resistance

ABSTRACT

Cancer resistance to chemotherapeutics is a common problem often encountered in the clinical setting, hampering greatly the conventional therapy of malignant diseases for several decades. No generally efficient mechanism solving this phenomenon was found so far. Cancer cells can adapt to a stress applied in the form of chemotherapeutics and become insensitive to their effects. Under such a selection pressure, the cancer cells acquire features helping them not only to survive the changes in the environment but also to further divide and to form secondary lesions. Therefore, besides developing novel chemotherapeutics, refining the drug delivery mechanisms of the conventional ones is absolutely crucial to defeat the cancer, so we can fully benefit from the effects these therapeutics offer. Here, we demonstrated enhanced delivery of doxorubicin (DOX) to a DOX-resistant ovarian cancer cell line using completely novel 2D material 4-carboxybutylgermanane (Ge-Bu-COOH). In our study, we present Ge-Bu-COOH as a drug carrier evincing high drug-loading efficiency, low cytotoxicity up to the concentration of 2.5 μg/mL and no hemolysis. Simultaneously, binding DOX to Ge-Bu-COOH increases DOX accumulation in the DOX-resistant cell lines. It leads to a significant anticancer efficiency enhancement in A2780/ADR DOX-resistant cell line; with the maximal effect reaching up to 62.8% compared to free DOX. These findings have profound influence on understanding the behaviour of doxorubicin-resistant tumours and open new horizon to manage their treatment.

1. Introduction

The extraordinary success of graphene and its analogues has stimulated extensive research in material chemistry aimed to discover other elementary two-dimensional (2D) materials beyond graphene. These intensive efforts resulted in a synthesis or rediscovery of many materials with unique properties including transition metal carbides and nitrides [1], transition metal dichalcogenides (TMDs) [2] or black phosphorus [3]. Several of them showed a potential in biomedical applications, especially in the area of drug targeting. [4-7] However, there are other promising materials still awaiting a thorough exploration of their properties and behaviour in the biological systems.

The ovarian cancer is responsible for around 2.5% of all malignancies in females. However, more alarming is that it accounts for around 5% of female cancer deaths. Besides other reasons as *e.g.* a late diagnosis caused by asymptomatic progression of the ovarian cancer, one of the leading causes of death is the development of a resistance to conventional therapy. [8] The ovarian cancer treatment consists of combination of a surgery with a chemotherapy, however, a relapse in these patients often occurs within first

Abbreviations: ADR, Adriamycin (=DOX tradename); DOX, doxorubicin; Ge-Bu-COOH, 4-carboxybutylgermanane; PGP, P-glycoprotein; RBCs, red blood cells; TMDs, transition metal dichalcogenides.

* Corresponding author.
E-mail address: pumera.group@gmail.com (M. Pumera).

https://doi.org/10.1016/j.apmt.2020.100697
2352-9407/

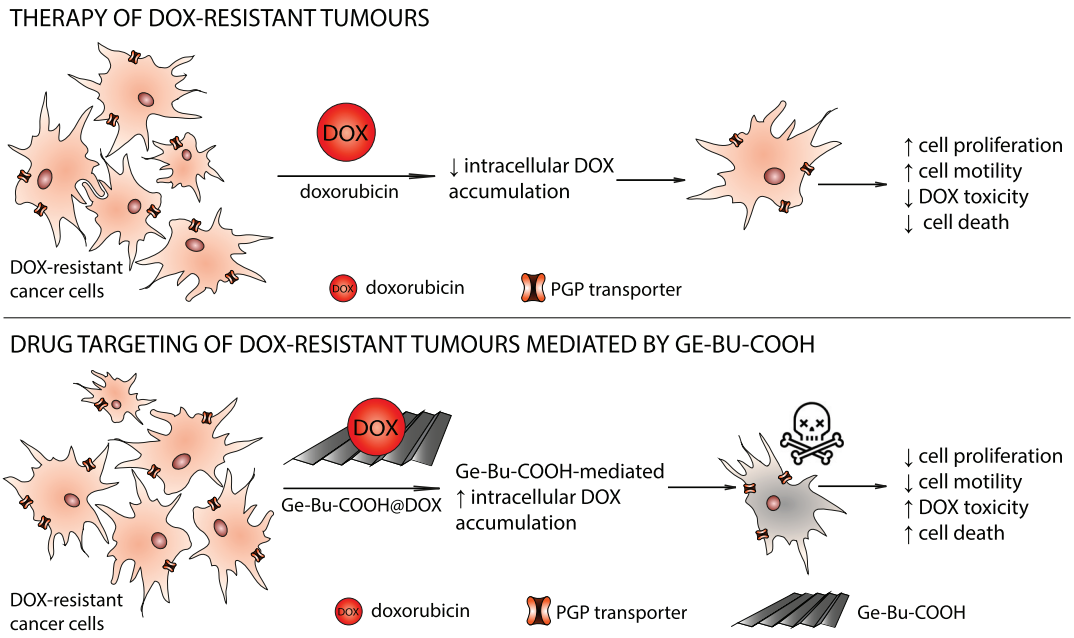

Scheme 1. Principle of Ge-Bu-COOH-mediated drug delivery in DOX-resistant cancer.

two years after the first therapeutic intervention. Standard first-line chemotherapy regimens are still evolving in order to achieve the highest efficiency and to overall benefit the patient. However, a development of the drug resistance is indisputably one of the key factors considerably reducing the chances for a patientś survival. [9] Several mechanisms responsible for a development of the drug resistance have been identified. These include the interpatient differences in drug pharmacokinetics [9, 10], a hypoxic tumour microenvironment affecting the cancer cell sensitivity, [9, 11] and more importantly, the specifics of the cancer cells themselves. [9] Besides other adaptive mechanisms of the cancer cells, the resistance is most frequently mediated by an overexpression of the drug efflux pumps from the ABC protein family. Under physiological circumstances, the ABC transporters are responsible for an ATP-dependent movement of various compounds across the cytoplasmatic membrane including xenobiotics, lipids, or metabolic products. [12] P-glycoprotein (PGP) is a member of the ABC transport protein family and its overexpression was found to be one of the key mechanisms of the cancer resistance. It is actively pumping the applied cytostatics out of the cell and thus decreasing their therapeutic efficiency. The PGP overexpression also hampers the therapeutic effects of one of the most widely used and most efficient chemotherapeutics - doxorubicin (DOX, trade name Adriamycin® (ADR), **Figure 1A**) and it is a leading cause of a development of the DOX-resistance in tumours. Binding DOX to nanocarriers allows to trick drug transport mechanisms and to modulate the therapeutic efficiency of the drug. A thorough assessment of novel micro- and nanomaterials is required, including their potential in the drug-targeting applications. DOX was selected in our study due to its wide employment in the clinical practice and because of its fluorescent properties enabling easy tracking of its accumulation. DOX accounts for one of the most widely prescribed and most potent anticancer agents ever developed. In the clinical setting, DOX is indicated against ovarian, breast, prostate and stomach cancer as well as against several types of haematological malignities. DOX is also often used in a combination with other antineoplastic agents. [13]

One of the youngest members of the graphene-like material family are group IV semiconductors, germanene and silicene. First theoretical studies reporting on the possibility of existence Si and Ge analogues of graphite were published in 1994 by Takeda *et al.* [14] followed by a study published by Cahangirov *et al.* in 2009 [15] These stable silicon and germanium 2D allotropes do not exist in nature and their synthesis was for a long time challenging. Unlike carbon atoms that prefer flat aromatic structure when forming the graphene structure, silicon and germanium atoms favour formation of the corrugated aromatic stage. [14] Germanene has a mixed sp^2 and sp^3 geometry leading to its nonplanar configuration. Its structure may be stabilized by hydrogenation resulting in the formation of hydrogenated germanene (GeH), also referred to as germanane [16] which stability may be even boosted by replacing the hydrogen atom with methyl groups. [17] The first successful synthesis of hydrogenated germanene $(GeH)_{2n}$ was described by Vogg *et al.* in 2000. [18] In comparison with pristine germanene, GeH evinces superior stability thanks to the lattice distortion which is absolutely essential for the prospective industrial applications. Those require also high-quantity production that was for GeH enabled after the employment of topochemical deintercalation of $CaGe_2$. [19]

Despite plenty of research activity around germanene and wide range of applications proposed for germanene-based materials during the last few years, there are still plenty of attractive areas to be explored. The potential of these materials in biological systems was, to the best of our knowledge, not described yet. In biomedical field, the potential of 2D materials was proven especially in the area of targeted drug delivery, particularly for transport of anticancer drugs. Several studies focused on an employment of germanene as a platform for the gas molecule attachment reported that it evinces higher chemical reactivity than graphene. [20] This was assigned to the germanene buckled honeycomb structure. Since similar reactivity might be expected with antineoplastic drugs, our goal was to evaluate germanane employment in the area of the drug delivery.

In our study, we prepared carboxylated derivative of germanane, 4-carboxybutylgermanane (Ge-Bu-COOH, see **Figure 1B**), and we focused on a comprehensive evaluation of its properties *in vitro*. We performed cytotoxicity evaluation of the pristine material on a panel of adherent cell lines derived from ovarian and prostate cancer tissue as well as its toxicity toward red blood cells (RBCs).

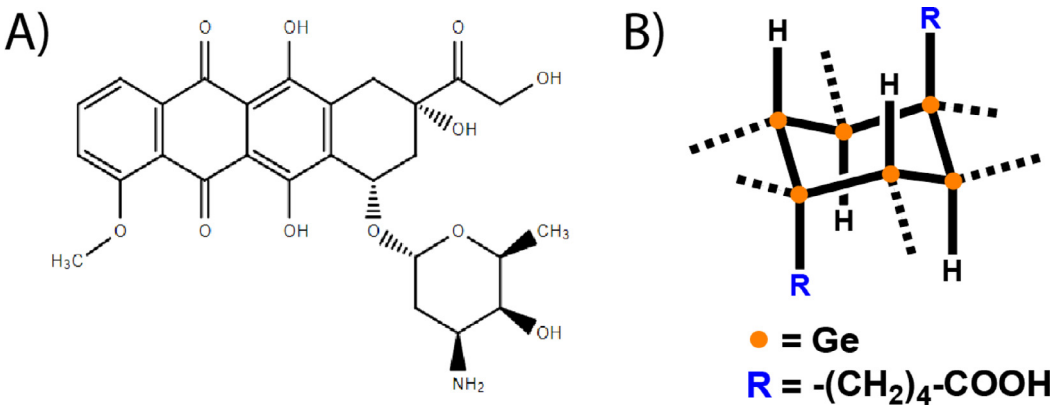

Figure 1. A) Structure of doxorubicin (DOX) and B) 4-carboxybutylgermanane (Ge-Bu-COOH).

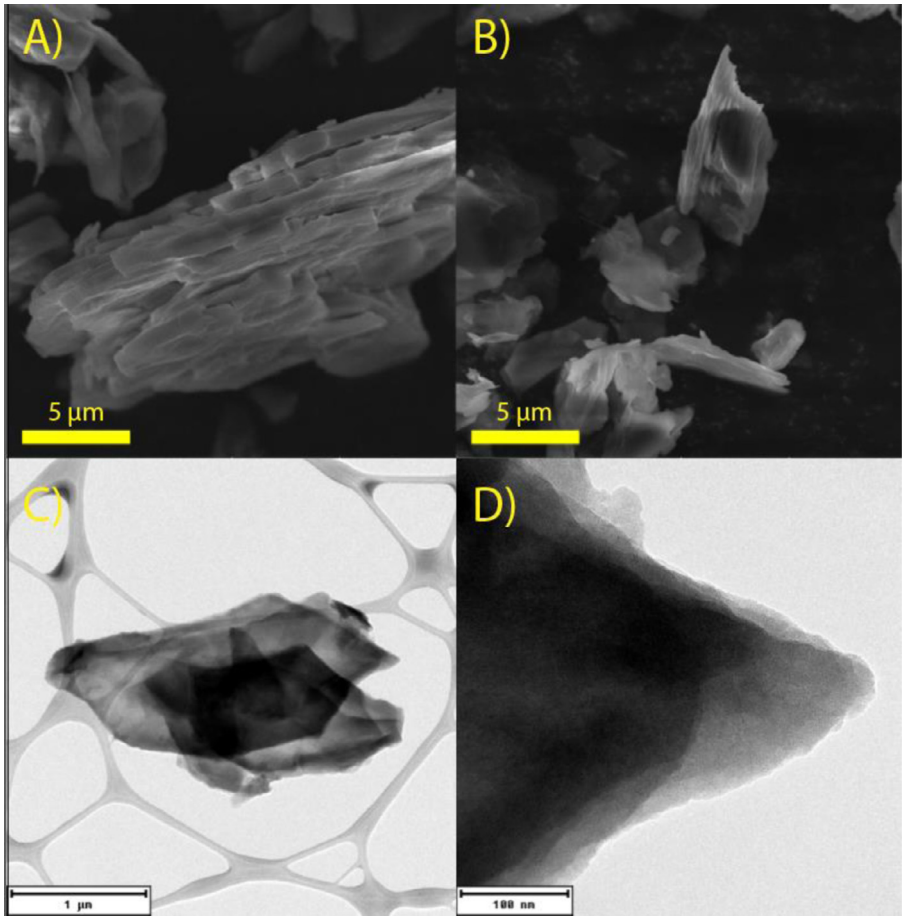

Figure 2. A), B) SEM images of Ge-Bu-COOH, C), D) TEM images of Ge-Bu-COOH nanosheets.

Further, the Ge-Bu-COOH potential in a targeted drug delivery of the antineoplastic drug DOX was explored, see **Scheme 1**. Among other cell lines, two ovarian cancer cell lines derived from the same tumour differing in their PGP status and endocytic potential were used; A2780 DOX-sensitive ovarian cancer cell line and A2780/ADR representing DOX-resistant ovarian cancer cell line. [21]. A binding efficiency of Ge-Bu-COOH nanosheets for DOX has been determined as well as the therapeutic efficiency *in vitro* and assessment of the DOX intracellular accumulation.

2. Results and Discussion

2.1. Synthesis and Characterization of Ge-Bu-COOH Nanosheets

The characteristic platelet morphology of Ge-Bu-COOH nanosheets is visible on the SEM images (**Figure 2A, 2B**). The individual sheets of the few-layered Ge-Bu-COOH are visible on the TEM images (**Figure 2C, 2D**). The elemental distribution (**Figure 3**) of Ge-Bu-COOH (**Figure 3A**) obtained by the energy-dispersive X-ray spectroscopy (EDS) shows homogeneous presence

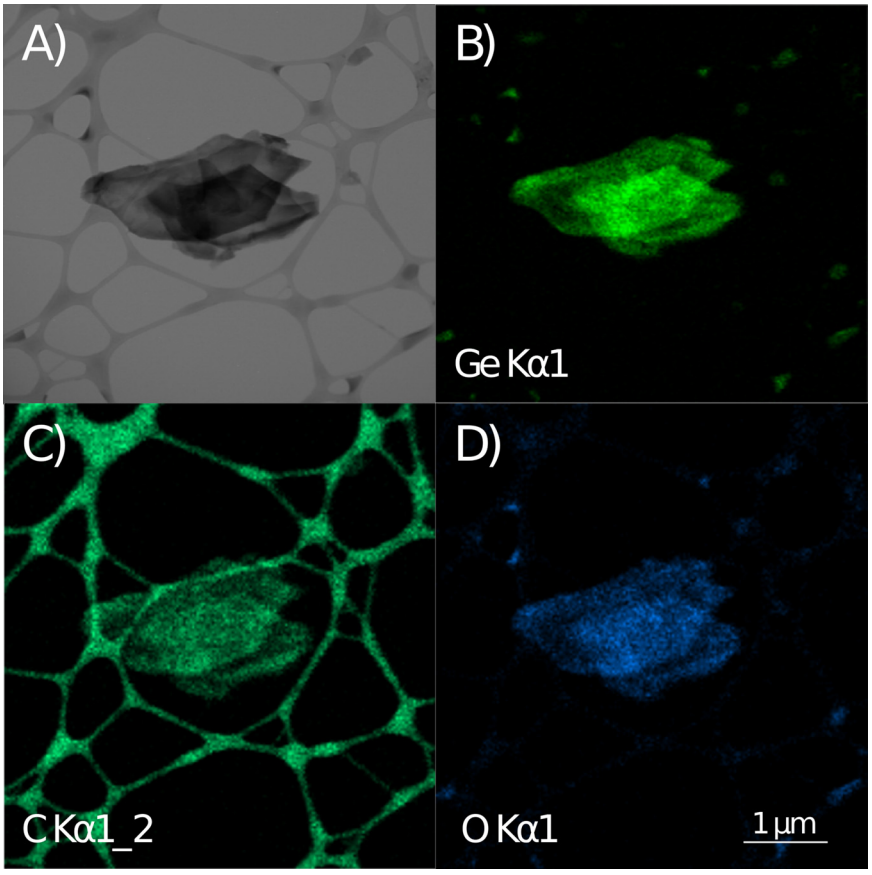

Figure 3. A) Ge-Bu-COOH TEM image and corresponding elemental distribution maps of B) Ge C) C, and D) O.

of germanium (**Figure 3B**) as well as carbon (**Figure 3C**) and oxygen (**Figure 3D**).

The chemical analysis was performed by XPS. The survey XPS spectrum (**Figure 4A**) shows the presence of germanium as well as of carbon and oxygen. The composition obtained from the XPS analysis shows 24.8 at.% Ge, 46.6 at.% C and 28.6 at.% O, which reflects the fact that approximately two alkyl groups are connected to the germanene skeleton composed of Ge_6 units and the rest four germanium atoms bear hydrogen ($Ge_6H_4R_2$ has theoretical composition 30 at.% Ge, 50 at.% C and 20 at.% O). The high-resolution XPS spectra of the individual main elements give clear evidence of the successful functionalization. The high-resolution Ge 3d spectrum is shown in **Figure 4B**. The maximum at 32.0 eV corresponds to Ge bound to carbon or hydrogen. In addition, minor peaks corresponding to elemental germanium at 28.4 eV and to germanium oxide from a surface oxidation at 34.1 eV can be seen. The high-resolution carbon C 1s spectrum (**Figure 4C**) shows the presence of C-C bonds at 285.0 eV originating from the alkyl functionalization as well as from the adventitious carbon contamination. The successful exfoliation and modification of germanane is confirmed by a peak at 283.1 eV, which corresponds to the Ge bound to carbon. The shoulder peak at 288.8 eV is clear evidence of presence of the COOH group, which terminates the alkyl chain connected to the germanane. In addition, the intensities of C 1s peaks are in the 8:1:1 ratio, which also confirms that one Ge-C bond corresponds to one COOH group. C-C peak is higher in intensity due to the presence of the adventitious carbon contamination. In addition, the high-resolution O 1s spectrum (**Figure 4D**) confirmed the presence of the COOH group as evident from the peak at 531.9 eV. The presence of a peak at 528.7 eV suggests oxidation of the germanane.

Particle size and surface zeta potential were determined by a dynamic light scattering (DLS) experiment. The average particle size obtained by DLS was 1230 nm (±71 nm) with surface zeta-potential of -22.1 mV (±2.0 mV), for details see **Table S1**. The negative zeta potential indicates a successful introduction of the carboxylic acid functionalities.

The Raman spectrum of the prepared material is shown in **Figure 5A** together with Raman spectrum of the starting $CaGe_2$. In the Raman spectrum of $CaGe_2$, the characteristic in-plane E_g vibrational mode is observed at 236 cm^{-1}. The respective E_2 in-plane mode of the exfoliated Ge-Bu-COOH was observed at 301 cm^{-1}, which also confirmed a successful chemical modification of germanane. Finally, the chemistry of the functionalized Ge-Bu-COOH was explored using FT-IR spectroscopy (**Figure 5B**). The vibration bands of the COOH groups are clearly visible at about 3300 cm^{-1} (O-H stretching mode) and 1730 cm^{-1} (C=O stretching mode) and C-H alkyl chain at about 2920 (C-H stretching mode) and 1400 cm^{-1} (C-H scissoring and C-H methyl rocking modes). A vibration band observed at 2000 cm^{-1} corresponds to a presence of the Ge-H bond (stretching mode), which is formed as a side product of $CaGe_2$ exfoliation with an alkyl halide.

2.2. Cytotoxicity of Ge-Bu-COOH

The cytotoxicity of the bare Ge-Bu-COOH nanosheets was assessed against a panel of ovarian and prostate cancer cell lines after their exposure to the material for 48 h, **Figure 6** and **Table 1**. For a 24 h treatment of the cells with Ge-Bu-COOH see **Figure S1** and **Table S2**. The applied concentration of the nanosheets ranged from 0 to 50 µg/mL. The median IC_{50} values were 6.5 µg/mL for the 24 h exposure and 3.65 µg/mL for the 48 h exposure. For the

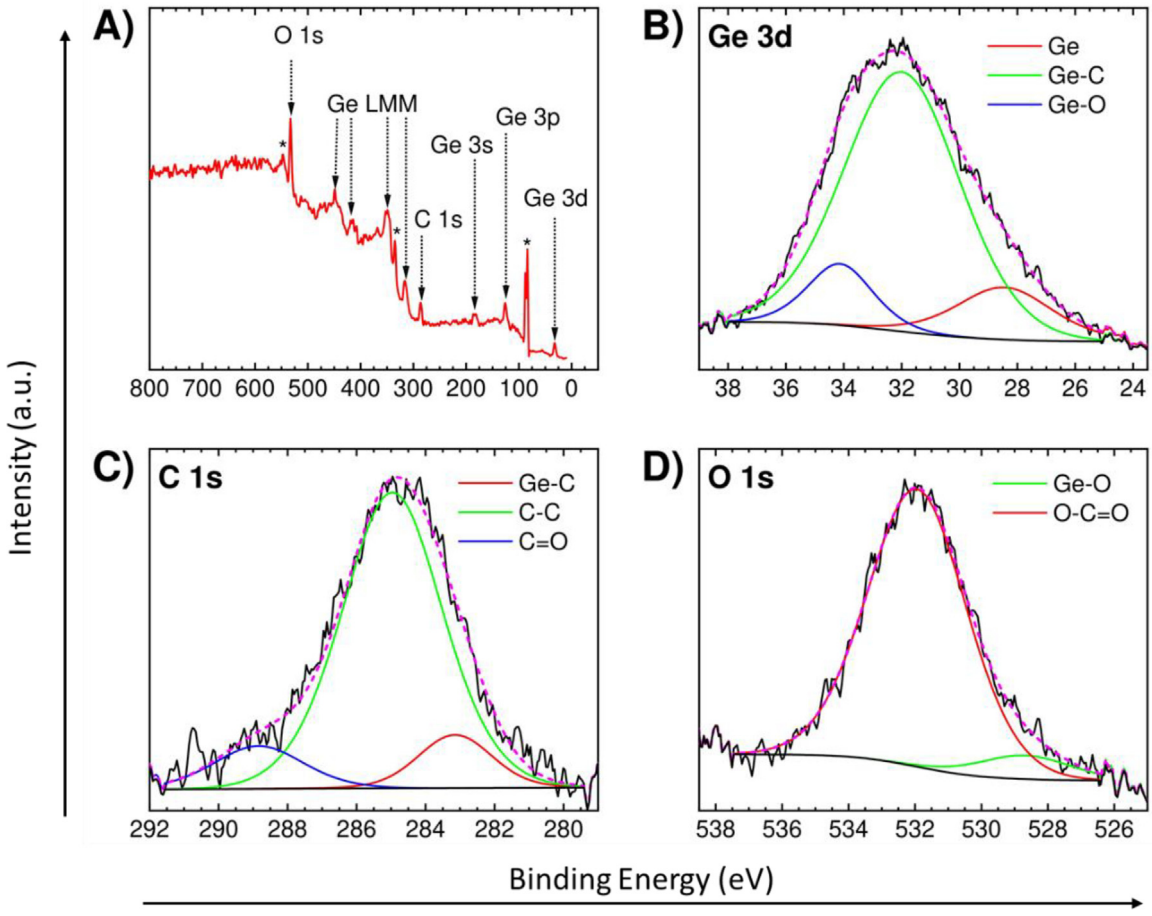

Figure 4. (A) XPS survey spectrum of 4-carboxybutylgermanane (Ge-Bu-COOH) and corresponding high-resolution spectra for (B) Ge 3d, (C) C 1s and (D) O 1s.

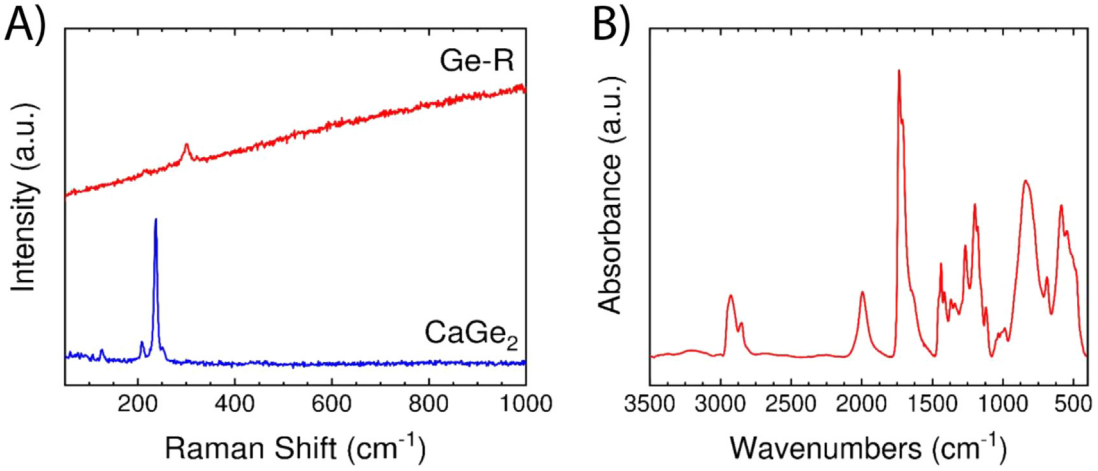

Figure 5. A) Raman spectra of Ge-Bu-COOH and $CaGe_2$ precursor, B) FT-IR spectra of Ge-Bu-COOH.

exact values see **Table 1** and **Table S2**. When determining the toxicity, a background correction was applied by subtracting the background signal of the Ge-Bu-COOH sheets, for the details see **Figure S2** and **Table S3**. The Ge-Bu-COOH nanosheets themselves are reducing 3-(4,5-dimethylthiazol-2-yl)-2,5-diphenyltetrazolium bromide, a dye used in the MTT viability assessment, and therefore, contribute to the measured signal. The same phenomenon was observed by our group in a previous study concerning the interference of black phosphorus nanoparticles with the tetrazolium dye. [7] This is of particular importance since in many studies published, background signal of the studied particles is neglected. That is the reason why in some studies concerning with the toxicity of 2D materials a sudden increase of cellular viability in the highest concentrations of the material is observed, even though there has been an evident trend of the materialś concentration-dependent toxicity. Ge-Bu-COOH is considered as non-toxic in the concentration range below 2.5–5 μg/mL in the case of a 24 h exposure. In the case of a 48 h exposure, depending on the type of the cell line tested generally concentrations below 2.5 μg/mL are considered as non-toxic with prostate tissue-derived cells being even more sen-

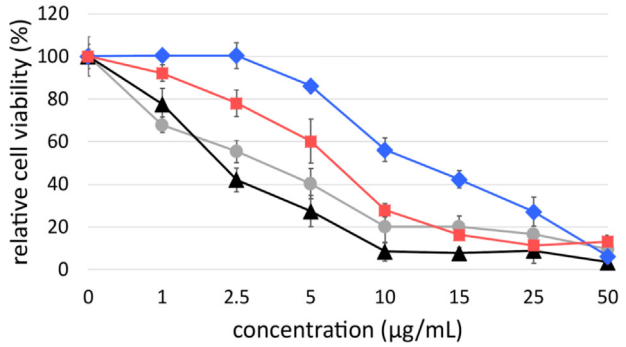

Figure 6. Relative viability of prostate cell lines: PNT1A (grey) and PC-3 (black), and ovarian cancer cell lines: A2780 (blue) and A2780/ADR (red) after 48 h treatment with Ge-Bu-COOH nanosheets. The x-axis represents Ge-Bu-COOH concentration ranging from 0 – 50 µg/mL, the y-axis represents the relative cell viability. Values are the average of three independent measurements performed in triplicates. Data are displayed as mean ± SD.

Table 1
Viability of selected cell lines after Ge-Bu-COOH exposure for 48 hours. Comparison of half-maximal inhibition concentration values (IC_{50}) for individual cell lines.

	48 h IC_{50} (μg/mL)
A2780	12.0 ± 2.3
A2780/ADR	4.9 ± 0.7
PC-3	2.4 ± 0.1
PNT1A	2.1 ± 0.6

sitive. In general, if the cell viability is not dropping under 80%, the concentration of the compound/material applied is considered as "non-toxic". After incubating Ge-Bu-COOH nanosheets with the cells for 24 h, a more dynamic cellular response was observed in the comparison with the 48 h cytotoxicity assessment. This is reflected in the relatively larger standard deviations of signals, for details see **Figure S1**.

2.3. Hemocompatibility of Ge-Bu-COOH

In order to evaluate a potential of Ge-Bu-COOH in biomedical applications, another parameter that needs to be determined is the material hemocompatibility, since most of these applications require an intravenous injection. *In vitro* blood compatibility was evaluated by incubating the concentrated red blood cells (RBCs) with Ge-Bu-COOH for 24 and 48 h followed by determination of the hemolysis degree. Surprisingly, in comparison with the toxicity of Ge-Bu-COOH towards adherent cells, high hemocompatibility was observed up to the highest Ge-Bu-COOH concentration tested. After applying the highest tested concentration of Ge-Bu-COOH (100 µg/mL), hemolysis accounted for around 2–3% and 5–6% after 24 h and 48 h of the exposure, respectively, **Figure 7A** and **7B**. This hematotoxicity is extremely low in comparison with the hematotoxicity of graphene oxide (GO) described by Liao et al. [22] In their study, they were actually concerning with the hematotoxicity of several types of graphene oxides (GO) towards erythrocytes. Here, the hemolysis was determined to be 75–90% for most types of GO particles after only 3 h incubation with 100 µg/mL of the nanosheets. The lowest hemolysis they observed was around 12.5%.

2.4. Loading of DOX on Ge-Bu-COOH

In general, 2D materials are characteristic with an extensive surface area that provides an unique platform for attaching various types of molecules including antineoplastic agents. [23] Large surface area is one of the key requirements necessary for an efficient drug loading. Many studies reported application of graphene [4, 24], graphene oxide [23, 25], TMDs [6, 26], or black phosphorus [27] in a targeted drug delivery. However, reports describing the ability of germanane-derived materials in this area are largely missing, even though its potential in this area is worth detailed exploration. Ge-Bu-COOH nanosheets (concentration 2.5 μg/mL) were incubated with 0 to 15 μM DOX for 24 and 48 h. Ge-Bu-COOH was dispersed in both PBS as well as in the culture medium to assess whether and how does the presence of proteins and other components of the cell culture medium affect the Ge-Bu-COOH binding ability of DOX. Ge-Bu-COOH binding efficiency (BE) was then calculated by measuring the fluorescence in the supernatant of the samples after their incubation with DOX, followed by a subsequent calculation of an amount of the material-bound DOX using its standard concentration curve. In the course of these experiments, two major observations have been made.

First, an incubation of Ge-Bu-COOH nanosheets with a cell culture medium greatly decreases its drug binding ability. The most evident difference was observed during the 24 h incubation where the decrease in BE appeared to be as high as 45% (2.5 μg/mL Ge-Bu-COOH, 1 μM DOX) when comparing the nanosheets incubated in the PBS and in the culture media. This is most likely caused by a formation of a material-protein complexes that are hampering DOX to bind to the nanosheets effectively. It is well known, that immediately after an introduction of nanosheets into physiological environment proteins bind to their surface and create so-called "protein corona". [28, 29] Protein corona is formed by proteins naturally occurring within the physiological system and its composition may vary depending on many factors. Those range naturally from the type of physiological condition in which the material was introduced, the type of the material itself, its size, shape, composition, or surface chemistry. Several studies reported that responses of a biological system to the introduction of particles are rather dependent on their surface area than on their mass. [28, 30] This might be particularly important for the 2D materials. Their extremely large surface-to-volume ratio implies that extensive protein corona formation on their surface might be expected. We assume that proteins present in the culture medium prevent DOX from binding to the materiaĺs surface because of the steric hindrances. We observed that higher DOX loading efficiency may be ensured by preincubating Ge-Bu-COOH nanosheets with DOX in PBS only, prior to an introduction of the nanosheets into the protein-rich environment, *e.g.* a culture medium or a bloodstream.

Second, we observed that an increased duration of the Ge-Bu-COOH incubation with the drug does not necessarily result in a more intensive surface binding. Depending on the DOX concentration applied, the 24 h incubation of Ge-Bu-COOH in culture medium evinced to lead to more efficient DOX binding on the surface of the nanosheets when compared with the 48 h incubation. The difference in BE between the 24 and 48 h incubation was reaching up to 33% (2.5 μg/mL Ge-Bu-COOH, 0.25 μM DOX), see **Figure 8** and **Table 2**. The binding efficiency of Ge-Bu-COOH (2.5 μg/mL) with DOX in PBS was found to be concentration-dependent reaching up to 66.4 % (1 μM DOX) after a 24 h incubation with agitation. An incubation extended over 48 h evinced drop in the BE across the whole concentration range. Simultaneously, a preincubation of Ge-Bu-COOH and DOX in a culture medium was found to significantly reduce the BE in both time points observed, rarely exceeding 20%; for details see **Figure S3** and **Table S4**.

2.5. Cytotoxicity of Ge-Bu-COOH Loaded with DOX

One of the main disadvantages of DOX anticancer therapy is the non-specificity of its anticancer effect which might lead to serious side effects towards the healthy tissues. The most serious condition patients undergoing DOX therapy might develop, is the DOX-associated cardiotoxicity. [31] This might, especially after ex-

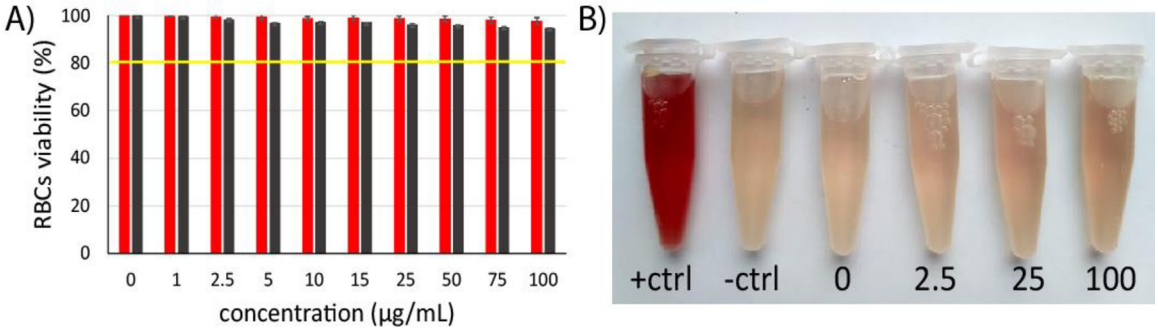

Figure 7. A) Hemocompatibility of Ge-Bu-COOH nanosheets. Viability of RBCs incubated with increasing concentration of Ge-Bu-COOH (0 – 100 µg/mL) for 24 (red) and 48 hours (black) at room temperature with agitation. Data represent mean ± SD of three measurements performed in triplicates. Yellow line highlights 80% viability considered in general as a threshold – below this value particles would not be considered as non-toxic. B) Hemolysis of RBCs after Ge-Bu-COOH exposure. Photographs of RBCs after 48h exposure to 0, 2.5, 25 and 100 μg/mL of nanosheets. The presence of red hemoglobin in the supernatant reflects membrane damage of RBCs. +ctrl and –ctrl represent positive and negative control, respectively.

Table 2
Binging efficiency (BE) of Ge-Bu-COOH in PBS. DOX BE (%) after incubation of Ge-Bu-COOH (2.5 μg/mL) with increasing drug concentration (μM).

c DOX (μM)	0	0.01	0.025	0.05	0.1	0.25	0.5	1	5	15
BE PBS 24 h (%)	0.0	14.6	11.2	21.0	28.6	45.0	55.6	66.4	44.2	26.8
BE PBS 48 h (%)	0.0	0.0	0.0	0.0	0.0	12.7	32.6	53.5	49.0	33.9

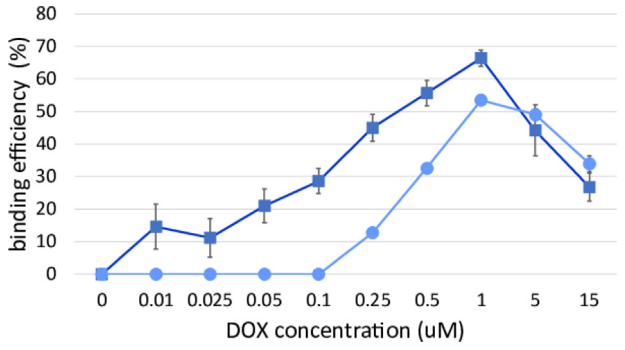

Figure 8. Binging efficiency (BE) of Ge-Bu-COOH in PBS. X-axis represents DOX concentration (μM) used for the incubation with Ge-Bu-COOH (2.5 μg/mL), the y-axis shows how much od DOX remained bound on the surface of the Ge-Bu-COOH after the 24 h (dark blue) and the 48 h (light blue) incubation followed by the double washing and by the centrifugation of the nanosheets. Data are shown as mean ± SD.

Table 3
Summary of the potentiation of DOX anticancer effect after binding it on the surface of Bu-Ge-COOH nanosheets. The data were collected for four cell lines (A2780, A2780/ADR, PNT1A, PC-3) in two timepoints (24 and 48 h). The average potentiation stands for the average of DOX anticancer effect improvement by binding it onto Bu-Ge-COOH nanosheets for all the concentration stated and for the individual cell line. Maximal potentiation stands then for the maximal increase of anticancer effect achieved.

	average potentiation (%)		maximal potentition (%)	
	24 h	48 h	24 h	48 h
A2780	7.5	-0.5	30.4	21.6
A2780/ADR	24.9	27.1	74.4	62.8
PC-3	22.6	7.7	49.1	30.4
PNT1A	22.1	11.9	34.5	23.0

ceeding the highest recommended cumulative dose of DOX, lead to the a congestive heart failure (CHF) manifesting 50% mortality. [32] Therefore, several mechanisms have been employed in order to overcome this scenario. These include, besides monitoring of the DOX cumulative dose administered to the patient, or administration of cardioprotective compounds, [33] also a targeting of its effect towards the cancer tissue using nanocarriers [34]. Here, since the DOX binding ability of Ge-Bu-COOH was proven, the same panel of ovarian and prostate cell lines was further used to determine the ability of Ge-Bu-COOH to transfer the therapeutic cargo and to deliver it to the site of action. Again, the non-toxic concentration of Ge-Bu-COOH (2.5 μg/mL) was used. The material was, similarly to previous experiment, incubated in PBS with an increasing concentration of DOX ranging from 0 to 15 μM for 24 h. We decided for a 24 h incubation as at the concentration of Ge-Bu-COOH was the BE for DOX higher than in the 48 h incubation experiment. After washing the unbound drug, Ge-Bu-COOH@DOX was resuspended in the cell culture medium (final concentration of Ge-Bu-COOH@DOX per well was again 2.5 μg/mL) and added to the cells. After incubation for 24 and 48 h, the efficiency of the drug targeting was assessed. Since similarly to Ge-Bu-COOH also Ge-Bu-COOH@DOX was a source of a significant interference, a background correction was used again.

Treatment of the cancer cells with Ge-Bu-COOH@DOX potentiated in overall anticancer effects of DOX in all the cells lines and in both time points. After 48 h, the anticancer effect of Ge-Bu-COOH@DOX in DOX-sensitive cell lines A2780, PNT1A, and PC-3 was in most concentrations stronger than when using DOX alone, see **Figure 9**. The highest potentiation of the anticancer effect achieved for A2780 cell line was 21.6% (15 μM DOX, 2.5 μg/mL Ge-Bu-COOH), for PNT1A cell line 30.4% (15 μM DOX, 2.5 μg/mL Ge-Bu-COOH), and for PC-3 cell line 23.0% (0.25 μM DOX, 2.5 μg/mL Ge-Bu-COOH). An exceptional potentiation of the DOX anticancer effect was observed after applying Ge-Bu-COOH@DOX on A2780/ADR cell line. Here, the DOX anticancer effect was increased by 62.8% after binding it onto the surface of Ge-Bu-COOH (15 μM DOX, 2.5 μg/mL Ge-Bu-COOH), for details see **Table 3**. Similar effect was observed after 24 h where the average potentiation of DOX anticancer effect was around 7.5% for A2780 cell line, 22.6% for PNT1A cell line and 22.1% for PC-3 cell line. Extraordinary potentiation was again achieved in A2780/ADR cell line where it reached on average 24.9% with maximum potentiation exceeding the 48 h effect when reaching up to 74.4%, see **Table 3**, **Figure S4**. In order to verify the data collected and to understand the exceptional potentiation of the DOX anticancer effect on a DOX-resistant

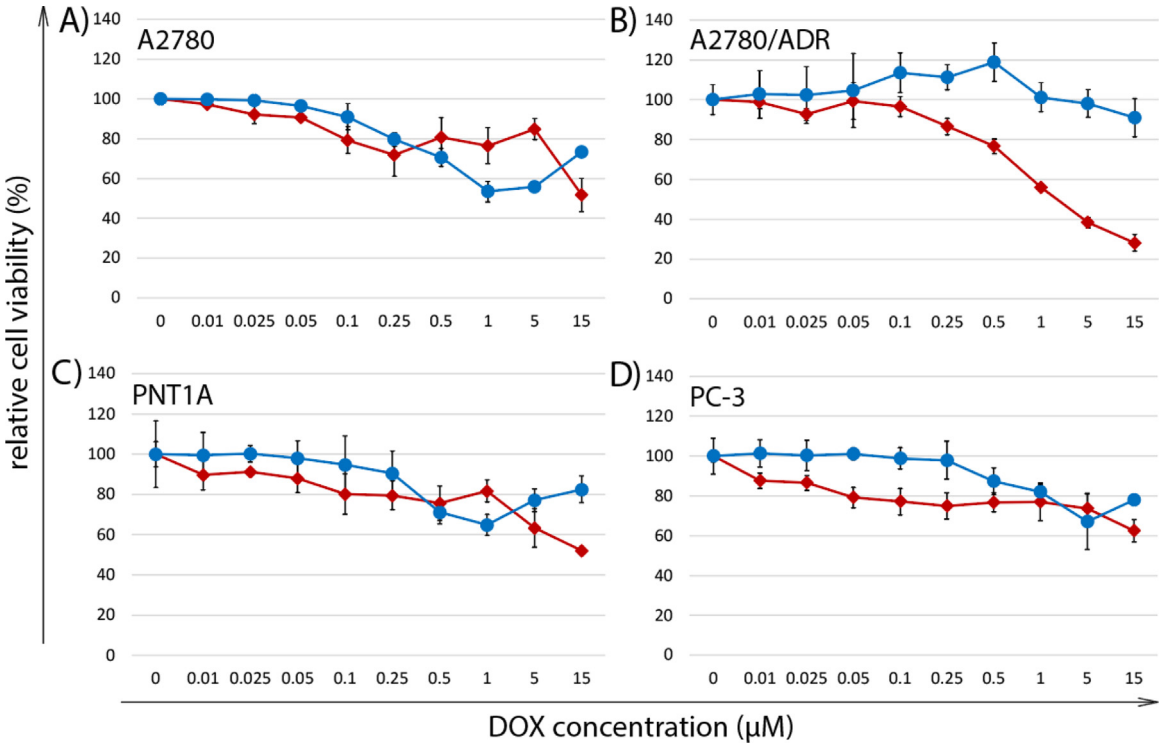

Figure 9. Relative viability of A) A2780, b) A2780/ADR, C) PNT1A, D) PC-3 cell lines after administration of DOX (blue) and Ge-Bu-COOH@DOX (red) for 48 h. The x-axis represents the DOX concentration and the y-axis represents the relative cell viability. In the case of Ge-Bu-COOH@DOX, the concentration of Ge-Bu-COOH nanosheets is constant across the DOX concentration range (2.5 μg/mL). Values are the average of four independent measurements. Data are displayed as mean ±SD.

cell line in the deeper context, fluorescence and holographic microscopy were further employed.

2.6. Cellular Uptake of Drug from Ge-Bu-COOH@DOX and DOX Distribution in Cells

Fluorescence microscopy was further employed to track the intracellular uptake and distribution of DOX released from Ge-Bu-COOH, see **Figure 10**. A2780 and A2780/ADR were selected for further experiments in order to explore the differences in the Ge-Bu-COOH@DOX response of DOX-sensitive and DOX-resistant cells. A2780 and A2780/ADR cells were treated for 6 and 48 h with Ge-Bu-COOH@DOX and the cell nuclei were subsequently stained with Hoechst 33342 (displayed in blue). In A2780 cells treated with Ge-Bu-COOH@DOX for 6 and 48 h, the intracellular incorporation of DOX (displayed in red) revealed a significant decrease with prolonged incubation time.

In general, the highest intensity of the fluorescence signal was found to be detected in the cytoplasm of both cell lines. A weak fluorescence signal was observed after 48 h treatment of A2780 cells with Ge-Bu-COOH@DOX in comparison with the fluorescence signal after 6 h. On the other hand, visible time-dependent increase in the DOX uptake was observed in A2780/ADR treated with Ge-Bu-COOH@DOX cells analysed at the same time points. These results confirm that A2780/ADR cell line evinces, in comparison with its DOX-sensitive counterpart, a different cellular response to the drug bound to Ge-Bu-COOH, manifested in the different drug uptake and its distribution in time. This in turn leads to the diverse spectrum of the responses to the drug applied and to the potentiation of DOX anticancer effect in A2780/ADR cell line.

2.7. Time-lapse holographic microscopy

Time-lapse holographic microscopy was employed to thoroughly evaluate the interaction of Ge-Bu-COOH and Ge-Bu-COOH@DOX with ovarian cancer cells A2780 and their DOX-resistant form A2780/ADR. Holographic microscopy enables a real-time monitoring, automatic cell segmentation, and quantitative measurements of morphological parameters of the cells without their staining or labelling. The obtained data are robust, collected under real conditions and enable to understand the observed processes in a deeper context. All the parameters were analysed based on the data recorded during 24 h experiments. First, an accumulation of bare Ge-Bu-COOH in both cell lines was assessed. Both cell lines evinced major accumulation of bare Ge-Bu-COOH nanosheets on the surface of the cells. A2780 cells were then showed to accumulate higher amount of the material when compared with A2780/ADR cells, for details see **Figure 11**.

Further, the collected data were compared with the administration of Ge-Bu-COOH@DOX (**Figure 12**). The impact of the Ge-Bu-COOH and Ge-Bu-COOH@DOX administration on the average cell mass was observed (**Figure 12A**). In this context, the cell mass reflects anabolic processes and active proteosynthesis, characteristic for the cell growth. The acquired data were found to be in an agreement with the results from the cytotoxicity assessment by MTT. After administration of 2.5 μg/mL of Ge-Bu-COOH, both cell lines were still proliferating, however, the A2780 cells evinced considerably higher proliferation rate (**Table 4**). Surprisingly, the administration of 2.5 μg/mL of Ge-Bu-COOH@DOX induced a significantly distinct cellular response in the used cell lines. The average cell mass of A2780 was rapidly increasing in the course of 24 h, while the proliferation rate of the resistant A2780/ADR cells was successfully decreased by Ge-Bu-COOH@DOX (**Table 4**). This confirms the potentiation of the DOX effect after its loading on Ge-Bu-COOH in A2780/ADR cells that are capable of evading its therapeutic effect under normal circumstances. The motility of A2780 and A2780/ADR significantly differs (**Figure 12B**). Under physiological conditions, the A24780/ADR cells evince higher motility which reflects their higher invasiveness. However, we observed that an ad-

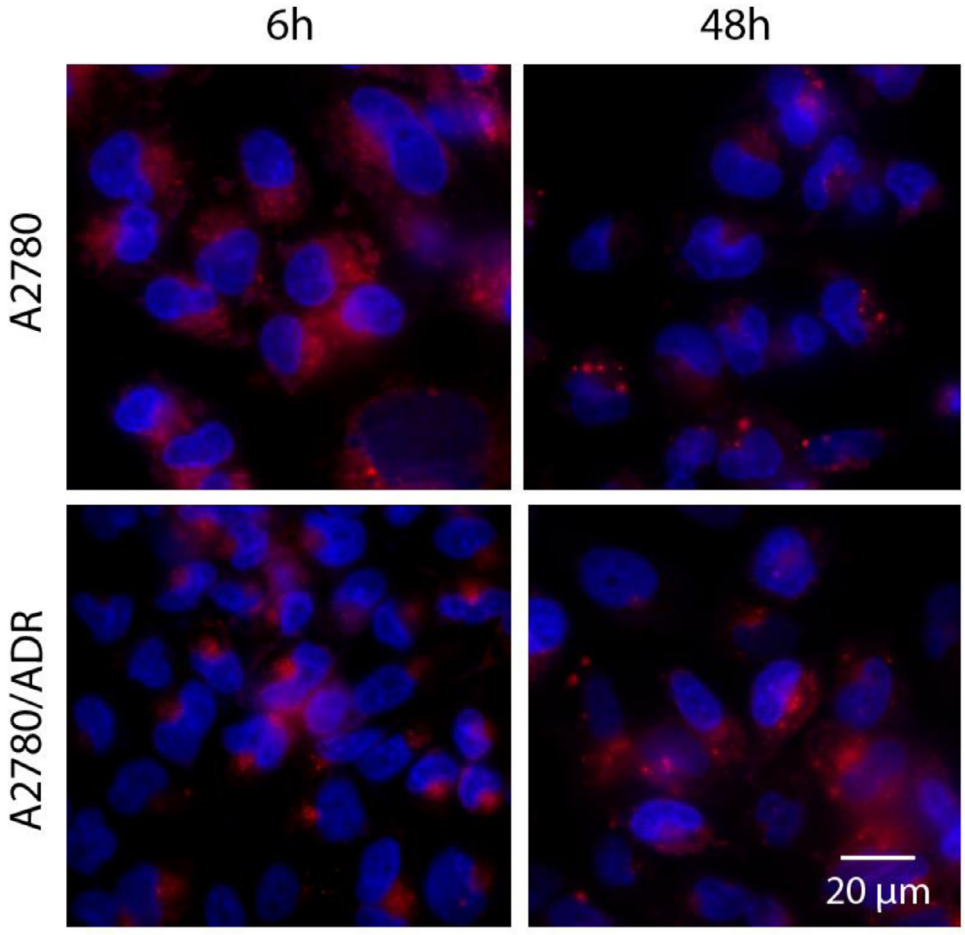

Figure 10. Intracellular distribution patterns of DOX delivered by Ge-Bu-COOH@DOX after 6 and 48 h incubation with A2780 and A2780/ADR cells. The blue channel represents fluorescence of Hoechst 33342-stained nuclei while the red channel represents the fluorescence of DOX. Scale bar 20 μm.

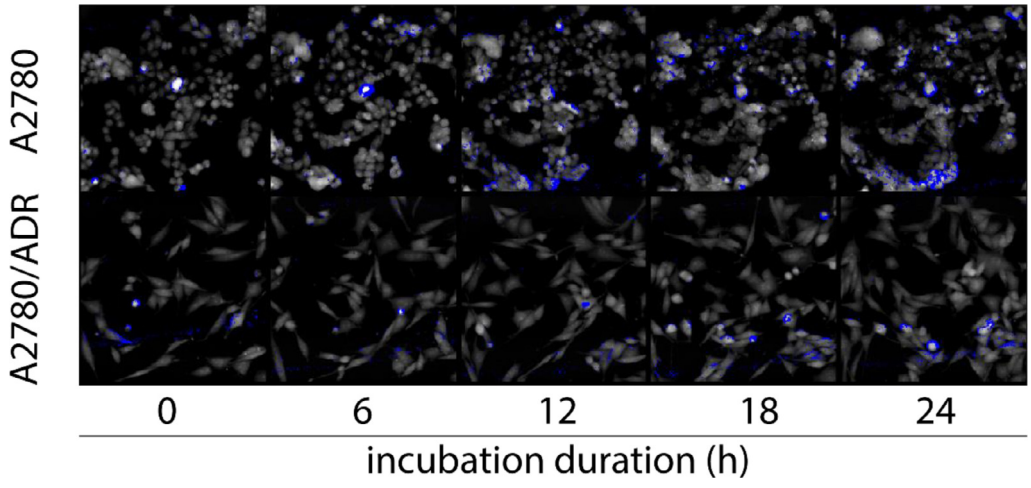

Figure 11. Colocalization experiment illustrating A2780 and A2780/ADR cells during the treatment with Ge-Bu-COOH (timepoints 0, 6, 12, 18, 24 h after Ge-Bu-COOH administration). Ge-Bu-COOH are visualised by blue colour.

Table 4
The proliferation of cells A2780 and A2780/ADR after administration of Ge-Bu-COOH and Ge-Bu-COOH@DOX expressed as a growth of the least square regression lines.

treatment vs. cells	rise of mean mass curve (pg/h)
2.5 μg/mL of Ge-Bu-COOH vs. A2780	3.041198954
2.5 μg/mL of Ge-Bu-COOH vs. A2780/ADR	0.191738757
2.5 μg/mL of Ge-Bu-COOH@DOX vs. A2780	5.227438339
2.5 μg/mL of Ge-Bu-COOH@DOX vs. A2780/ADR	-1.353703237

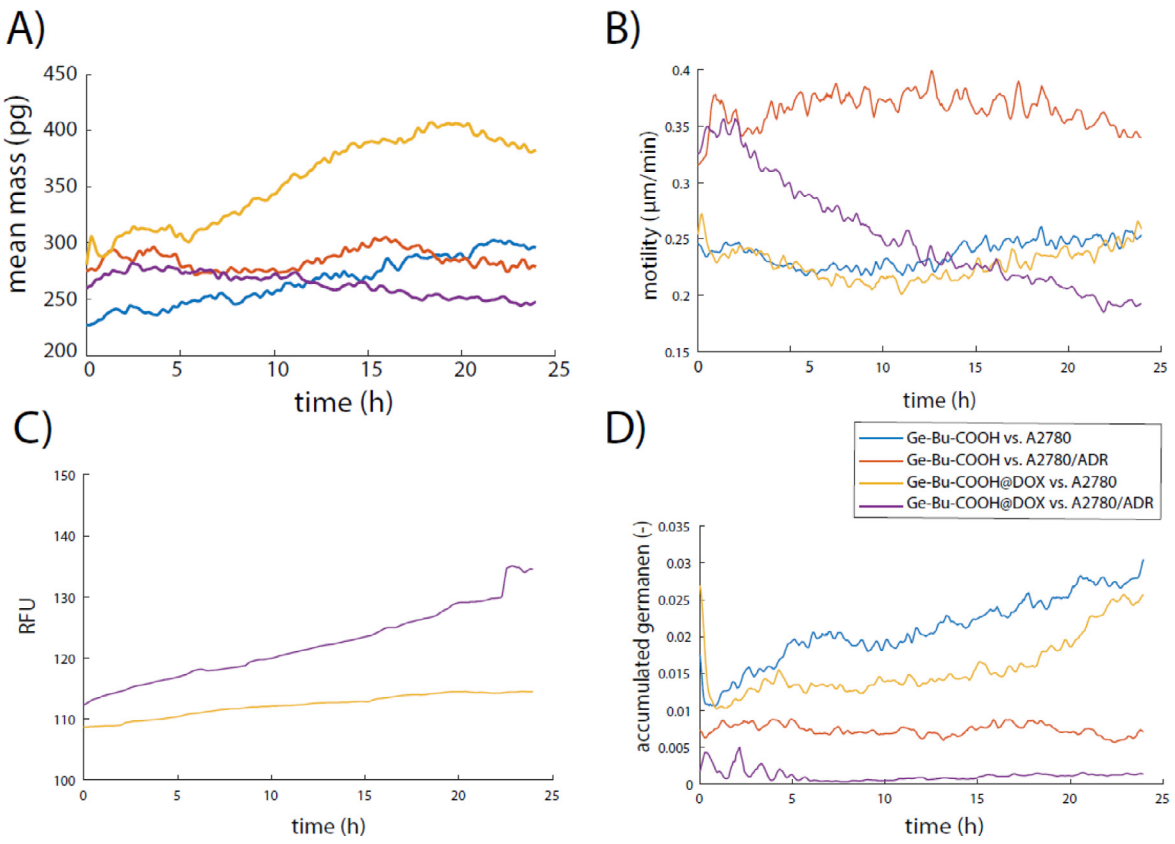

Figure 12. Quantitative phase time-lapse imaging of A2780 and A2780/ADR cells after administration of 2.5 μg/mL of Ge-Bu-COOH and 2.5 μg/mL of Ge-Bu-COOH@DOX. Evaluated parameters: A) average cell mass, B) average cell motility, C) DOX fluorescence after administration of Ge-Bu-COOH@DOX expressed in relative fluorescence units (RFU), D) accumulated Ge-Bu-COOH and Ge-Bu-COOH@DOX.

ministration of 2.5 μg/mL of Ge-Bu-COOH@DOX greatly suppresses their velocity (**Figure 13**) and therefore, this might prevent them from spreading and also potentially from forming secondary lesions, *e.g.* metastases.

Quantitative phase imaging (QPI) with fluorescence digital holographic microscopy was used in order to evaluate the DOX accumulation in both cell lines after application of Ge-Bu-COOH@DOX (**Figure 12C**). While in A2780 just a slight increase of fluorescence was recorded in the course of time, the resistant subtype A2780/ADR manifested a steady significant increase in the DOX accumulation within 24 h, which is in an agreement with the data acquired by the fluorescence microscopy (**Figure 10**). This also explains the greater cytotoxicity of the Ge-Bu-COOH-mediated DOX delivery for A2780/ADR determined by the cytotoxicity assays. In A2780 cells, contrarily to the poor DOX uptake delivered by Ge-Bu-COOH, A2780 cells considerably accumulate Ge-Bu-COOH nanosheets (**Figure 12D**) while no accumulation was observed in the A2780/ADR cells within the monitored period of time. This implies that Ge-Bu-COOH can make the A2780/ADR cells accumulate more DOX while actually not accumulating within the cells itself. We assume, that Ge-Bu-COOH might bind to the cellular surface, mechanically block the PGP pump and thus prevent the cells from pumping the drug out. As a result, the A2780/ADR cells accumulated more DOX which is under normal circumstances pumped out of the cells by the overexpressed PGP. We found that if we block these pumps mechanically with Ge-Bu-COOH, DOX remains trapped within the cells and induces extensive cellular death of the cancer cells. Therefore, a superior therapeutic effect of DOX bound to Ge-Bu-COOH might be observed in A2780/ADR over A2780.

3. Conclusion

In this work, we have reported on the synthesis of 4-carboxybutylgermanane (Ge-Bu-COOH) nanosheets for a targeted delivery of the anticancer drug doxorubicin (DOX) to DOX-resistant cancer cells. The cytotoxicity assessments revealed low toxicity of Ge-Bu-COOH up to the concentration 2.5 μg/mL—a concentration sufficient for an efficient DOX binding. The DOX loading on the surface of Ge-Bu-COOH nanosheets enabled its delivery to the malignant cells. In DOX-sensitive cells, it potentiated its therapeutic effect *in vitro* on average by up to 22.6%. An exceptional therapeutic effect was observed in the DOX-resistant A2780/ADR ovarian cancer cell line. Here, the cytotoxicity of DOX after its loading on Ge-Bu-COOH surface was improved on average by up to 27.1% with the highest potentiation reaching 62.8% for 48 h treatment and 74.4% for 24 h treatment. DOX potentiation leading to intensive cancer cell death was further proved also by fluorescent and holographic microscopy. Our study demonstrates a unique potential of Ge-Bu-COOH as a bio- and hemocompatible nanocarrier suitable for refining and enhancing the therapeutic efficiency of the conventional cancer treatment. Besides, our study provides new insights into the design of new Ge-Bu-COOH-based systems for versatile biomedical applications.

4. Experimental Section

Synthesis of 4-carboxybutylgermanane: Calcium (99%) and germanium (99.999%) were obtained from Alfa, Germany. Methyl 5-bromopentanoate was obtained from Fluorochem, Great Britain. Potassium iodide, potassium carbonate, acetone, hydrochloric acid

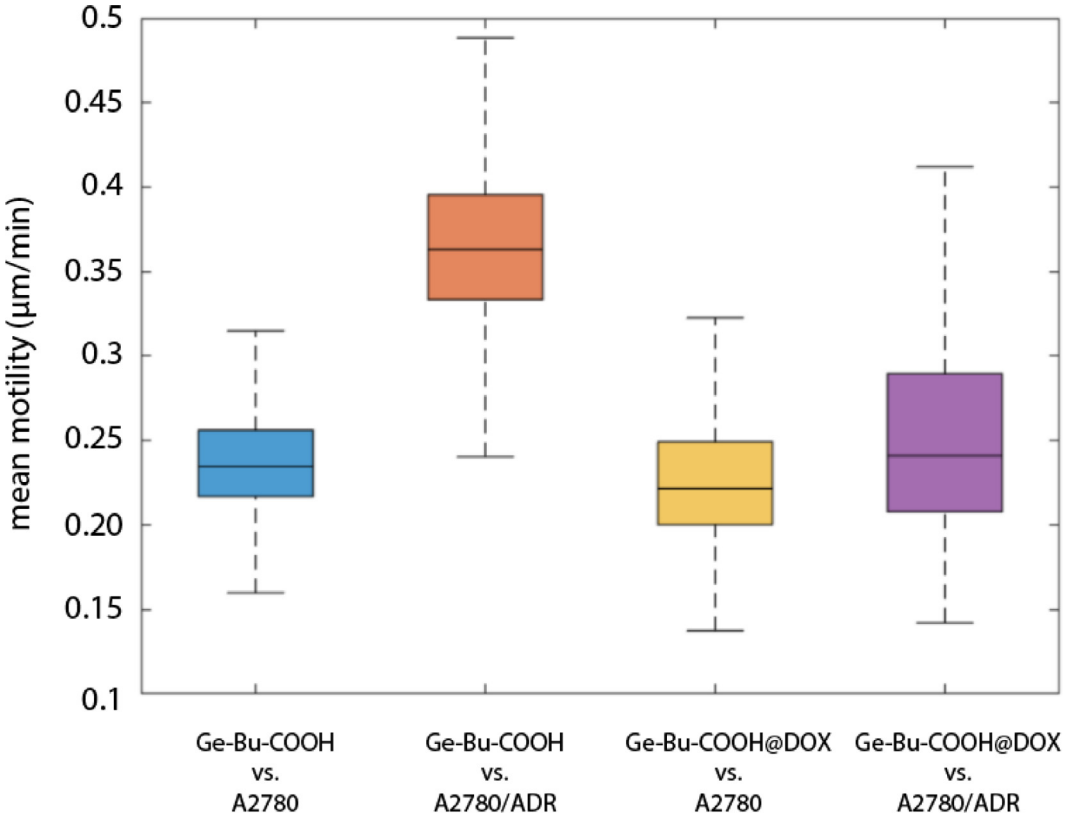

Figure 13. Box and whiskers graph of motility of A2780 and A2780/ADR cells after administration of Ge-Bu-COOH and Ge-Bu-COOH@DOX.

(37%) were obtained from Penta, Czech Republic. Calcium germanide was made by direct reaction from elements in a quartz ampoule with an alumina liner. Stoichiometric amount of calcium and germanium corresponding to 10 g of $CaGe_2$ was heated at 1000°C for 10 h and cooled on room temperature using 1°C/min cooling rate. Calcium germanide (200 mg) was placed into a sintered glass funnel and methyl 5-bromopentanoate (5 mL) and potassium iodide (3 g) were added. Water was added to reach the bottom of the sintered glass and the mixture was left at room temperature for 5 days. The product was collected by filtration, washed with water (5 × 50 mL) and acetone (3 × 50 mL). 1M aqueous potassium carbonate (30 mL) was added and the mixture was stirred overnight at room temperature, collected by filtration and washed with water (2 × 50 mL). 0.5 M aqueous hydrochloric acid (50 mL) was added and the mixture was stirred for 2 h at room temperature. The solid was collected by filtration, washed with water (5 × 50 mL) and acetone (2 × 50 mL). The solid was dried in vacuo and stored in dark under an inert argon atmosphere.

Material characterization: A field-emission scanning electron microscope (SEM; TESCAN MAIA 3) was used get take the images of the morphology of the material. Transmission electron microscopy (TEM) was performed using an EFTEM Jeol 2200 FS microscope (Jeol, Japan) with 200 keV acceleration voltage used for the measurement. The elemental maps were acquired with an SDD detector X-MaxN 80 TS from Oxford Instruments (England). The sample was prepared by drop casting a suspension of the nanosheets (1 mg/mL in water) on a TEM grid (Cu; 200 mesh; Formvar/carbon) and dried at 60°C for 12 h. X-Ray photoelectron spectra (XPS) of the samples were acquired using a SPECS spectrometer equipped with XR 50 MF X-Ray source and Phoibos 150 CCD hemispherical analyzer operating at constant pass energy (80 eV for the survey and 40 eV for the high-resolution spectra). The Al Kα radiation (1486.6 eV) was used for excitation of the electrons. The samples were placed on a conductive carrier made from a gold-coated silicon wafer piece. InVia Raman microscope (Renishaw, England) in a backscattering geometry with a CCD detector was used for Raman spectroscopy. DPSS laser (532 nm, 50 mW) with applied power 5 mW and 50x magnification objective were used for the measurement. The peak of a silicon reference sample at 520 cm^{-1} was used to calibrate the instrument. Resolution of the spectra was less than 1 cm^{-1}. The samples were suspended in deionized water (1 mg/mL) and ultrasonicated for 10 min. The suspension was deposited on a small piece of a silicon wafer and dried. An iS50R FTIR spectrometer (Thermo Scientific, USA) was used for the FT-IR experiments. The measurement was performed in a reflectance mode using the built-in diamond ATR with direct deposition of the Ge-Bu-COOH sample onto the surface of the diamond. The dynamic light scattering (DLS) experiment was performed using a Zetasizer Nano ZS (Malvern, England). The measurement was performed at room temperature (20°C) using a glass cuvette. The measurements of the zeta-potential were performed on a Malvern Zetasizer Nano ZS. The measurement was performed at pH = 7.0 in 50 mM PBS solution. A suspension of sample concentration 1 mg/mL in PBS was used for the measurement.

Chemical and biochemical reagents: Fetal bovine serum (FBS) (mycoplasma-free), penicillin-streptomycin, and trypsin were purchased from PAA Laboratories GmbH (Pashing, Austria). Doxorubicin solution (2 mg/mL) was purchased from Teva Pharmaceuticals (Prague, Czech Republic). RPMI-1640 medium, Ham's F12 medium, phosphate-buffered saline pH 7.2 (PBS), MTT reagent, ethylenediaminetetraacetic acid (EDTA), dimethyl sulfoxide (DMSO), and all other chemicals of the ACS purity were purchased from Merck (Darmstadt, Germany), unless otherwise noted.

Cell line and cell culture: A panel of cancerous and non-cancerous cell lines was used to comprehensively evaluate the effect of Ge-Bu-COOH on the targeting and on the therapeutic ef-

ficiency of DOX. The discrimination of the material-bound drugs between a healthy and a malignant tissue was further assessed using PNT1A and PC-3 cells. The PNT1A cells represent a non-cancerous human epithelial prostate cell line, while the PC-3 cells were established from the bone metastasis of the human prostate cancer. The potential of the Ge-Bu-COOH-bound DOX to overcome the mechanism of the drug-resistance was evaluated on a set of ovarian cancer cells. The A2780 human cancer cell line was established from tumour tissue of an untreated patient with ovarian cancer. Further, its Adriamycin-resistant subline (A2780/ADR) was subjected to the toxicity assessment in order to investigate whether the Ge-Bu-COOH-bound DOX has any potential to overcome the difficulties associated with their resistance to the conventional treatment. Cell lines were purchased from Health Protection Agency Culture Collections (Salisbury, UK). All the cell lines were cultivated in RPMI-1640 medium, only PC-3 cell line was grown in Ham's F12 medium. The Adriamycin-resistant cells A2780/ADR were treated with 10^{-7} M DOX once a week according to the supplier's instructions. Cell culture media were supplemented with 10% FBS and with antibiotics (penicillin 100 U/mL and streptomycin 0.1 mg/mL). The cells were grown in an incubator at 37°C in a humidified 5% CO_2 mixture with ambient air.

Preparation of Ge-Bu-COOH: Prior to every use, Ge-Bu-COOH was sonicated in PBS (Ge-Bu-COOH stock solution concentration 0.1 mg/mL) for 120 minutes. For the Ge-Bu-COOH-mediated drug targeting, a material concentration 2.5 μg/mL was selected since it was previously confirmed as the highest concentration yet non-toxic across the panel of tested cell lines (see **Figure 6**).

MTT cytotoxicity of Ge-Bu-COOH: The cells were seeded on a 96-well plate at a density ensuring 70% confluence in the day of the treatment (A2780—13000 cells/well, A2780/ADR—12000 cells/well, PC-3 8000 cells/well, PNT1A 10000 cells/well). The cells were grown in a culture medium, incubated at 37 °C in a humidified 5% CO_2 atmosphere. After 48 h, the medium was removed and replaced with a fresh culture medium containing Ge-Bu-COOH in concentration ranging from 0 to 100 µg/mL (200 μL per well). After 24 and 48 h of the treatment, the cell culture medium was removed again, and the cells were incubated with a fresh medium containing 1 mg/mL of MTT reagent (200 µL per well) for another 4 h. Plates with the cells were kept in a humidified atmosphere at 37 °C, wrapped in an aluminium foil. After that, the medium with MTT was replaced with 99.9% DMSO (200 μL per well) to dissolve the formazan crystals. Then, glycine buffer (25 μL per well) was added to DMSO, gently shaken, and the absorbance at 570 nm was read. The absorbance was in this and in all the biological experiments mentioned further determined using Cytation 3 Imaging reader (BioTek Instruments, Winooski, WT, USA). Since in the absorbance read Ge-Bu-COOH was a source of significant interference in the absorbance read, a background subtraction was performed (see **Figure S2** and **Table S3** for details). The IC_{50} values were then calculated by fitting the data with the logistic function to create a sigmoidal dose-response curve. All measurements were performed in tetraplicates.

Hemolysis Assay: A fresh erythrocyte concentrate was obtained from St. Anne's University Hospital (Brno, Czech Republic). The concentrated red blood cells (RBCs) were diluted by calcium- and magnesium-free Dulbecco's phosphate-buffered saline (DPBS) to the concentration of around $5\bullet10^8$ cells/mL. To test the hemolytic activity of Ge-Bu-COOH, RBC suspension (0.2 mL, around 10^8 cells) was added to a suspension of Ge-Bu-COOH in DPBS (0.8 mL). The final Ge-Bu-COOH concentrations ranged from 0 to 100 μg/mL. D.I. water (+RBCs) and DPBS (+RBCs) were used as the positive and negative control, respectively. All the samples were placed on a rocking shaker and incubated for 24 and 48 h. The hemoglobin absorbance in the supernatant was measured at 540 nm, with 655 nm as a reference. A degree of the hemolysis was calculated using Equation 1:

$$hemolysis(\%) = \left(\frac{sample\ abs_{540-655\ nm} - negative\ ctrl\ abs_{540-655\ nm}}{positive\ ctrl\ abs_{540-655\ nm} - negative\ ctrl\ abs_{540-655\ nm}} \right) x100 \quad (1)$$

Loading of DOX on Ge-Bu-COOH: The loading of DOX on the surface of Ge-Bu-COOH was initiated by the sonication of the nanosheets in PBS (Ge-Bu-COOH stock solution concentration 0.1 mg/mL) for 120 minutes. For the Ge-Bu-COOH-mediated drug targeting, material concentration 2.5 μg/mL was selected since it was previously confirmed as the highest non-toxic concentration across the panel of the tested cell lines (see **Figure 6**). After that, we incubated the nanosheets with an increasing concentration of DOX ranging from 0 to 15 μM for 24 or 48 h. After incubation, samples were twice centrifuged (2 °C, 9000 rpm, 60 min) and washed with PBS. After the last centrifugation, the Ge-Bu-COOH@DOX samples were resuspended in PBS, or a culture medium according to the requirements of the subsequent experiment.

Ge-Bu-COOH efficiency of DOX binding: Ge-Bu-COOH (2.5 μg/mL) was incubated with an increasing concentration of DOX (0–15 μM) in PBS as well as in culture medium for 24 and 48 h. Ge-Bu-COOH binding efficiency (BE) was then calculated by measuring the fluorescence in the supernatant of these samples. After removing the nanosheets by centrifugation (2 °C, 9000 rpm, 60 min), DOX fluorescence in the supernatants was excited at 475 nm and the emission was detected using a 580 nm bandpass emission filter (Cytation 3 Imaging reader, BioTek Instruments, Winooski, WT, USA). The percentage of DOX bound onto the surface of Ge-Bu-COOH, *e.g.* the binging efficiency (BE) was determined by relating it to the data acquired by fluorescence measurement (475 excitation, 580 nm emission) of the free DOX in the same concentration range in both, PBS and the culture medium (RPMI as well as Ham's F12 culture media) using the same spectrophotometer. Ge-Bu-COOH drug binding efficiency (BE) was calculated using Equation 2:

$$BE(\%) = \left(100 - \frac{A_{Ge-Bu-COOH@DOX} - 100}{A_{DOX}} \right) \quad (2)$$

where $A_{Ge\text{-}Bu\text{-}COOH@DOX}$ represents the absorbance of the supernatant removed after the centrifugation of Ge-Bu-COOH with DOX and A_{DOX} represents the absorbance of the DOX solution at the same concentration the material was initially incubated with. For the calculation of Ge-Bu-COOH BE in PBS, a calibration curve of DOX in PBS was used. For the calculation of Ge-Bu-COOH BE in cell culture medium, a calibration curve of DOX in the cell culture medium was used.

Cytotoxicity of Ge-Bu-COOH loaded with DOX: As with our previous experiment, a panel of cell lines was used to determine any possible combinatory anticancer effects of Ge-Bu-COOH and DOX. The cells were seeded on a 96-well plate at a density ensuring 70% confluence in the day of the treatment (A2780—13000 cells/well, A2780/ADR—12000 cells/well, PC-3 8000 cells/well, PNT1A 10000 cells/well). Ge-Bu-COOH (2.5 μg/mL) was incubated with an increasing concentration of DOX (0–15 μM) in PBS for 24 h. After the incubation, Ge-Bu-COOH@DOX was centrifuged (2°C, 9000 rpm, 60 min), washed twice with PBS, resuspended in culture medium (final concentration of Ge-Bu-COOH@DOX per well was 2.5 μg/mL) and added to the cells. The plates were then incubated in at 37 °C in a humidified 5% CO_2 atmosphere. After the incubation for 24 and 48 h, the cell culture medium was removed and replaced with a fresh medium containing MTT reagent (1 mg/mL). The plates with the cells were kept in a humidified atmosphere at 37 °C,

wrapped in an aluminium foil. After that, the medium with MTT was exchanged with 99.9% DMSO (200 μL per well) to dissolve the formazan crystals. Then, glycine buffer (25 μL per well) was added to DMSO, gently shaken, and the absorbance was read at a wavelength of 570 nm. Since Ge-Bu-COOH was a source of a significant interference, a background subtraction of Ge-Bu-COOH@DOX in the cell culture medium was performed. The IC_{50} values were then calculated by fitting the data with the logistic function to create a sigmoidal dose-response curve. All measurements were performed in tetraplicates.

Cellular uptake and distribution of DOX in cells: The cellular uptake and distribution of DOX and Ge-Bu-COOH@DOX were assessed by fluorescence microscopy (Nikon Eclipse Ti-S, Nikon Instruments Inc., USA) for both A2780 and A2780/ADR cell lines. The cells were seeded into ibiTreat $I^{0.8}$ μ-Slide Luer chambers (ibidi, Martinsried, Germany). After incubation for 4 days, the cell culture medium was replaced by a fresh medium containing: 30 nM DOX or Ge-Bu-COOH@DOX suspension (2.5 μg/mL Ge-Bu-COOH incubated for 24 h with 15 μM DOX, incubation followed by double centrifugation and double washing of the nanosheets with PBS). After 6, 12, 24, and 48 h, the cells were washed twice with fresh culture medium and subsequently stained with Hoechst 33342. The untreated cells stained in the same way were used as a control. The cells were analysed using a fluorescence microscope with excitation/emission wavelengths 350/480 nm for Hoechst 33342 and 480/570 nm for DOX. The images were captured using a Nikon camera (Nikon Digital Sight DS-Ri2) and analysed by FIJI software. [35]

Holographic microscopy: Quantitative phase imaging (QPI) of the living cells was performed using Q-PHASE, a coherence-controlled holographic microscope, CCHM (TELIGHT, Brno, Czech Republic). The microscopic setup is based on an off-axis holography and incorporates a diffraction grating allowing imaging with both, spatially and temporally low-coherent illumination leading to high-quality QPI. [36] After seeding the A2780 and A2780/ADR cells into ibiTreat $I^{0.8}$ μ-Slide Luer chambers (ibidi, Martinsried, Germany) and incubation for 48 h, the cell culture medium was replaced by a fresh medium containing: Ge-Bu-COOH (2.5 μg/mL in culture medium) or Ge-Bu-COOH@DOX suspension (2.5 μg/mL of Ge-Bu-COOH incubated for 24 h with 15 μM DOX, incubation followed by a double centrifugation and a double washing of the nanosheets with PBS). The time-lapse monitoring was performed for 24 h at a frame rate 1 frame/3 min. For holographic observations, Nikon Plan 10x/0.3 was used, the interferograms for holography were taken using a CCD camera (XIMEA MR4021MC). The fluorescence mode used a solid-state light source (Lumencor Aura II) and a sCMOS camera (Andor Zyla 5.5, 2560 $\times$ 2160 px) was used to capture the images. Numerical reconstruction is needed to process the raw holographic data and is performed by a Q-PHASE control software. This software implements established methods of fast Fourier-transformation and phase unwrapping. The amplitude image and the unwrapped phase image is the output from the software, where the phase image has high intrinsic contrast and may be processed by an available image processing software and the amplitude image can be used for the segmentation of Ge-Bu-COOH/Ge-Bu-COOH@DOX. Images were analysed using MATLAB custom script. Cells were segmented in the phase images using specialized QPI segmentation method proposed by Loewke *et al.* [37] Ge-Bu-COOH/Ge-Bu-COOH@DOX was segmented by simple thresholding of the amplitude images. The amount of accumulated Ge-Bu-COOH/Ge-Bu-COOH@DOX was calculated from the overlay of cells and Ge-Bu-COOH/Ge-Bu-COOH@DOX areas as a percentage of the area of the cells covered by the Ge-Bu-COOH/Ge-Bu-COOH@DOX. Cell tracking for motility calculation was performed by simple nearest neighbour search (in time) with respect to Intersection over Union (IoU) of segmentation masks, where everything with IoU smaller than 0.7 were discarded as segmentation error and not used for the motility calculation.

Author Contributions

The manuscript was written through contributions of all authors. All authors have given approval to the final version of the manuscript. M.F. conceived the idea, received comments and edits from all the authors, designed the experiments, monitored the research and performed, analysed, or assisted in all the biological experiments; J.B. performed holographic and fluorescent microscopy; M.R. helped with in vitro experiments and data interpretation; T.V. analysed the data obtained by holographic microscopy; J.S., Z.S., J.P., and J.L. performed the synthesis and characterisation of 4-carboxybutylgermanane; M.M. and M.P. initiated and supervised the study. All authors contributed to the writing of their corresponding sections.

Notes

The authors declare no competing financial interests.

Conflict of interests

Authors declare no conflict of interests.

Credit statement

The manuscript was written through contributions of all authors. All authors have given approval to the final version of the manuscript. M.F. conceived the idea, received comments and edits from all the authors, designed the experiments, monitored the research and performed, analysed, or assisted in all the biological experiments; J.B. performed holographic and fluorescent microscopy; M.R. helped with in vitro experiments and data interpretation; T.V. analysed the data obtained by holographic microscopy; J.S., Z.S., J.P., and J.L. performed the synthesis and characterisation of 4-carboxybutylgermanane; M.M. and M.P. initiated and supervised the study. All authors contributed to the writing of their corresponding sections.

Acknowledgment

M.P. acknowledges the financial support of Grant Agency of the Czech Republic (EXPRO: 19-26896X). M.M. was supported by the project “Center for Tumor Ecology – Research of the Cancer Microenvironment Supporting Cancer Growth and Spread” (reg. no. CZ.02.1.01/0.0/0.0/16_019/0000785) supported by the Operational Program Research, Development and Education. Z. S. was further supported by the Neuron Foundation. M.F. was further supported by funds from the Faculty of Medicine MU to junior researcher.

Supplementary materials

Supplementary material associated with this article can be found, in the online version, at doi:10.1016/j.apmt.2020.100697.

References

[1] J.B. Pang, R.G. Mendes, A. Bachmatiuk, L. Zhao, H.Q. Ta, T. Gemming, H. Liu, Z.F. Liu, M.H. Rummeli, Chemical Society Reviews 48 (2019) 72–133 C. N. R. Rao, K. Pramoda, Bulletin of the Chemical Society of Japan 2019, 92, 441-468.
[2] K. Kalantar-zadeh, J.Z. Ou, T. Daeneke, M.S. Strano, M. Pumera, S.L. Gras, Advanced Functional Materials 25 (2015) 5086–5099.
[3] R. Gusmao, Z. Sofer, M. Pumera, Angewandte Chemie-International Edition 56 (2017) 8052–8072.
[4] J.Q. Liu, L. Cui, D. Losic, Acta Biomaterialia 9 (2013) 9243–9257.

[5] K. Yang, S.A. Zhang, G.X. Zhang, X.M. Sun, S.T. Lee, Z.A. Liu, Nano Letters 10 (2010) 3318–3323 Y. Yong, L. J. Zhou, Z. J. Gu, L. Yan, G. Tian, X. P. Zheng, X. D. Liu, X. Zhang, J. X. Shi, W. S. Cong, W. Y. Yin, Y. L. Zhao, Nanoscale 2014, 6, 10394-10403.
[6] T. Liu, C. Wang, X. Gu, H. Gong, L. Cheng, X.Z. Shi, L.Z. Feng, B.Q. Sun, Z. Liu, Advanced Materials 26 (2014) 3433–3440.
[7] M. Fojtu, X.Y. Chia, Z. Sofer, M. Masarik, M. Pumera, Advanced Functional Materials 27 (2017) 7.
[8] L.A. Torre, B. Trabert, C.E. DeSantis, K.D. Miller, G. Samimi, C.D. Runowicz, M.M. Gaudet, A. Jemal, R.L. Siegel, Ca-a Cancer Journal for Clinicians 68 (2018) 284–296.
[9] R. Agarwal, S.B. Kaye, Nature Reviews Cancer 3 (2003) 502–516.
[10] L. Iyer, M.J. Ratain, European Journal of Cancer 34 (1998) 1493–1499.
[11] A. Tomida, T. Tsuruo, Anti-Cancer Drug Design 14 (1999) 169–177.
[12] J.I. Fletcher, M. Haber, M.J. Henderson, M.D. Norris, Nature Reviews Cancer 10 (2010) 147–156.
[13] C. Sauter, Lancet 342 (1993) 1550–1551 J. Gehl, M. Boesgaard, T. Paaske, B. V. Jensen, P. Dombernowsky, Seminars in Oncology 1996, 23, 35-38.
[14] K. Takeda, K. Shiraishi, Physical Review B 50 (1994) 14916–14922.
[15] S. Cahangirov, M. Topsakal, E. Akturk, H. Sahin, S. Ciraci, Physical Review Letters 102 (2009) 4.
[16] a) C.J. Rupp, S. Chakraborty, J. Anversa, R.J. Baierle, R. Ahuja, Acs Applied Materials & Interfaces 8 (2016) 1536–1544. I. Gablech, J. Pekarek, J. Klempa, V. Svatos, A. Sajedi-Moghaddam, P. Neuzil, M. Pumera, Trac-Trends In Analytical Chemistry 2018, 105, 251-262, DOI: 10.1016/j.trac.2018.05.008.
[17] a) S.S. Jiang, S. Butler, E. Bianco, O.D. Restrepo, W. Windl, J.E. Goldberger, Nature Communications 5 (2014) 6. J. Sturala, J. Luxa, S. Matějková, J. Plutnar, T. Hartman, M. Pumera, Z. Sofer, Chem. Mater. 2019, 31(24), 10126-10134, DOI: 10.1021/acs.chemmater.9b03391; c) J. Sturala, J. Luxa, S. Matějková, Z. Sofer, M. Pumera, Nanoscale 2019, 35002, DOI: 10.1039/C9NR04081A d) N. F. Rosli; N. Rohaizad; J. Sturala; A. C. Fisher; R. D. Webster; Martin Pumera, Adv. Funct. Mater, 2020, in press https://doi.org/10.1002/adfm.201910186.
[18] G. Vogg, M.S. Brandt, M. Stutzmann, Advanced Materials 12 (2000) 1278 -+.
[19] Nana Liu, Guyue Bo, Yani Liu, Xun Xu, Yi Du, X. Dou, Shi, Small (2019) M. Houssa, E. Scalise, K. Sankaran, G. Pourtois, V. V. Afanas'ev, A. Stesmans, Applied Physics Letters2011, 98, 3.
[20] U. Srimathi, V. Nagarajan, R. Chandiramouli, Applied Surface Science 475 (2019) 990–998 V. Nagarajan, R. Chandiramouli, Superlattices and Microstructures 2017, 101, 160-171; V. Nagarajan, R. Chandiramouli, Journal of Molecular Liquids 2017, 234, 355-363.
[21] H.C. Arora, M.P. Jensen, Y. Yuan, A.G. Wu, S. Vogt, T. Paunesku, G.E. Woloschak, Cancer Research 72 (2012) 769–778 A. M. Rogan, T. C. Hamilton, R. C. Young, R. W. Klecker, R. F. Ozols, Science 1984, 224, 994-996; J. T. Drummond, A. Anthoney, R. Brown, P. Modrich, Journal of Biological Chemistry 1996, 271, 19645-19648.
[22] K.H. Liao, Y.S. Lin, C.W. Macosko, C.L. Haynes, Acs Applied Materials & Interfaces 3 (2011) 2607–2615.
[23] L.M. Zhang, J.G. Xia, Q.H. Zhao, L.W. Liu, Z.J. Zhang, Small 6 (2010) 537–544.
[24] M. Mahdavi, F. Rahmani, S. Nouranian, Journal of Materials Chemistry B 4 (2016) 7441–7451.
[25] X.Y. Yang, X.Y. Zhang, Z.F. Liu, Y.F. Ma, Y. Huang, Y. Chen, Journal of Physical Chemistry C 112 (2008) 17554–17558 T. Zhou, X. M. Zhou, D. Xing, Biomaterials 2014, 35, 4185-4194.
[26] W. Yang, L. Gan, H.Q. Li, T.Y. Zhai, Inorganic Chemistry Frontiers 3 (2016) 433–451 Z. Y. Lei, W. C. Zhu, S. J. Xu, J. Ding, J. X. Wan, P. Y. Wu, Acs Applied Materials & Interfaces 2016, 8, 20900-20908.
[27] W.S. Chen, J. Ouyang, H. Liu, M. Chen, K. Zeng, J.P. Sheng, Z.J. Liu, Y.J. Han, L.Q. Wang, J. Li, L. Deng, Y.N. Liu, S.J. Guo, Advanced Materials 29 (2017) 7 W. Tao, X. B. Zhu, X. H. Yu, X. W. Zeng, Q. L. Xiao, X. D. Zhang, X. Y. Ji, X. S. Wang, J. J. Shi, H. Zhang, L. Mei, Advanced Materials 2017, 29, 10.
[28] P. Aggarwal, J.B. Hall, C.B. McLeland, M.A. Dobrovolskaia, S.E. McNeil, Advanced Drug Delivery Reviews 61 (2009) 428–437.
[29] T. Cedervall, I. Lynch, S. Lindman, T. Berggard, E. Thulin, H. Nilsson, K.A. Dawson, S. Linse, Proceedings of the National Academy of Sciences of the United States of America 104 (2007) 2050–2055.
[30] D.M. Brown, M.R. Wilson, W. MacNee, V. Stone, K. Donaldson, Toxicology and Applied Pharmacology 175 (2001) 191–199 K. Donaldson, D. Brown, A. Clouter, R. Duffin, W. MacNee, L. Renwick, L. Tran, V. Stone, Journal of Aerosol Medicine-Deposition Clearance and Effects in the Lung 2002, 15, 213-220; C. L. Tran, D. Buchanan, R. T. Cullen, A. Searl, A. D. Jones, K. Donaldson, Inhalation Toxicology 2000, 12, 1113-1126.
[31] C.C. Lim, C. Zuppinger, X.X. Guo, G.M. Kuster, M. Helmes, H.M. Eppenberger, T.M. Suter, R.L. Liao, D.B. Sawyer, Journal of Biological Chemistry 279 (2004) 8290–8299.
[32] K. Chatterjee, J.Q. Zhang, N. Honbo, J.S. Karliner, Cardiology 115 (2010) 155–162.
[33] A.R.L. Ludke, A. Al-Shudiefat, S. Dhingra, D.S. Jassal, P.K. Singal, Canadian Journal of Physiology and Pharmacology 87 (2009) 756–763.
[34] S. Rivankar, Journal of Cancer Research and Therapeutics 10 (2014) 853–858.
[35] J. Schindelin, I. Arganda-Carreras, E. Frise, V. Kaynig, M. Longair, T. Pietzsch, S. Preibisch, C. Rueden, S. Saalfeld, B. Schmid, J.Y. Tinevez, D.J. White, V. Hartenstein, K. Eliceiri, P. Tomancak, A. Cardona, Nature Methods 9 (2012) 676–682.
[36] B. Gal, M. Vesely, J. Collakova, M. Nekulova, V. Juzova, R. Chmelik, P. Vesely, Plos One 12 (2017) 14.
[37] N.O. Loewke, S. Pai, C. Cordeiro, D. Black, B.L. King, C.H. Contag, B. Chen, T.M. Baer, O. Solgaard, Ieee Transactions on Medical Imaging 37 (2018) 929–940.